Heterojunction-Mediated Catalysis

DOI: 10.1002/anie.201404481

Nanojunction-Mediated Photocatalytic Enhancement in Heterostructured CdS/ZnO, CdSe/ZnO, and CdTe/ZnO Nanocrystals**

*Clive Eley, Tong Li, Fenglin Liao, Simon Michael Fairclough, Jason M. Smith, George Smith, and Shik Chi Edman Tsang**

Abstract: *A series of highly efficient semiconductor nanocrystal (NC) photocatalysts have been synthesized by growing wurtzite-ZnO tetrahedrons around pre-formed CdS, CdSe, and CdTe quantum dots (QDs). The resulting contact between two small but high-quality crystals creates novel CdX/ZnO heterostructured semiconductor nanocrystals (HSNCs) with extensive type-II nanojunctions that exhibit more efficient photocatalytic decomposition of aqueous organic molecules under UV irradiation. Catalytic testing and characterization indicate that catalytic activity increases as a result of a combination of both the intrinsic chemistry of the chalcogenide anions and the heterojunction structure. Atomic probe tomography (APT) is employed for the first time to probe the spatial characteristics of the nanojunction between cadmium chalcogenide and ZnO crystalline phases, which reveals various degrees of ion exchange between the two crystals to relax large lattice mismatches. In the most extreme case, total encapsulation of CdTe by ZnO as a result of interfacial alloying is observed, with the expected advantage of facilitating hole transport for enhanced exciton separation during catalysis.*

Zinc oxide (ZnO) is a widely investigated material for the photodecomposition of organic pollutants and toxic contaminants in air and water.[1–4] However, overcoming poor quantum yields caused by fast internal exciton recombination[5] is a severe limitation in realizing the high catalytic activity necessary for commercially viable applications. Several approaches have been investigated to improve ZnO catalytic activity, including both cation[6] and anion[7] doping, metal–semiconductor Schottky junctions,[8–10] surface decoration with organic molecules,[11] and morphology manipulations.[12,13] Recent work has focused on creating multiphase or "heterostructured" semiconductor systems, such as ZnO/CdSe,[14] ZnO/CuS,[15] ZnO/SnO_2,[16] ZnO/CdTe,[17] and ZnO/CdS,[18] which are composites of ZnO and other semiconductors with suitably matched band energy. The rationale is that type-II interfaces between semiconductors causes spatial separation and increased lifetimes of photogenerated excitons, which reduces internal charge recombination and increases catalytic activity.[19] To date, the synthesis of these systems has involved the deposition of a second semiconductor phase onto pre-formed ZnO nanocrystals (NCs). To our knowledge, this work is the first example of a series of high-quality heterostructured photocatalysts prepared by growing ZnO NCs around pre-formed cadmium chalcogenide quantum dots (QDs) using a simple and scalable solution-based approach. We report the successful growth of ZnO tetrahedrons around colloidal CdS, CdSe, and CdTe QDs, which give rise to novel type-II heterostructured semiconductor nanocrystals (HSNCs) with significantly increased photocatalytic activity relative to pure ZnO. In performing a comparative study across a series of chalcogenides, we observe that the rate of exciton generation, and hence photocatalytic activity, is related to both the nature of the chalcogenide anion and the structure of the junction between the different semiconductors. Atomic probe tomography (APT) yields unprecedented insight into nanojunction structure, revealing increasing degrees of interfacial ion exchange (CdS < CdSe < CdTe) proportional to material softness and inversely proportion to lattice mismatch. We observe that CdS and CdSe NCs form extensive but sharp material interfaces when located on the surface of ZnO crystals, but the much softer CdTe NCs with highest lattice mismatch generate more extensive ion exchange with ZnO, leading to total encapsulation by the ZnO crystalline phase. Thus, we demonstrate the possibility of establishing an internal CdTe/ZnO nano-interface that can significantly modify the photocatalytic properties of ZnO without photocorrosion of CdTe and its potential leaching into solution.

CdS, CdSe, and CdTe QDs, with average diameters of 5.4, 3.0, and 3.7 nm respectively, were synthesized according to the method of Peng and Peng,[20] and then used as seed NCs for ZnO overgrowth. The as-synthesized QDs exhibited distinctively broad XRD crystalline peaks corresponding to wurtzite-CdS, wurtzite-CdSe, and zinc blende-CdTe NCs (Figure S3, Supporting Information), and first excitonic absorption peaks at $\lambda = 452$, 548, and 606 nm, respectively (Figure S4), indicating strong quantum confinement effects.

[*] C. Eley, F. Liao, Dr. S. M. Fairclough, Prof. S. C. E. Tsang
Wolfson Catalysis Centre, Department of Chemistry
University of Oxford
Oxford OX1 3QR (UK)
E-mail: edman.tsang@chem.ox.ac.uk
Dr. T. Li,[+] Dr. J. M. Smith, Prof. G. Smith
Department of Material Science, University of Oxford
Oxford OX1 3PH (UK)
[+] Present address: Australian Center for Microscopy and Microanalysis, The University of Sydney
Sydney, NSW 2006, Australia)

[**] This research was supported by The Rhodes Trust and EPRSC doctoral prize funding. TEM was performed by University of St Andrews (UK) through the EPSRC access scheme.

Supporting information for this article is available on the WWW under http://dx.doi.org/10.1002/anie.201404481.

ZnO NCs were synthesized from a zinc acetate precursor at 300 °C based on the method of McLaren et al.[12] Whether grown in the absence or presence of the seed QDs, the resulting single-crystal ZnO NCs were tetrahedral in shape with sharp crystal edges and diameters between 50–100 nm.

When grown in the presence of the QDs, the ZnO tetrahedrons were in direct contact with the CdS, CdSe, and CdTe phases (Figure 1). The composition, by weight, of the resulting HSNCs based on yield calculations is approximately 10 % CdX (X = S, Se, Te) to approximately 90 % ZnO. Closer TEM examination revealed that for both the CdS/ZnO and CdSe/ZnO samples, smaller (5–15 nm) spherical CdS and CdSe NCs decorate the surface of larger (50–100 nm) ZnO tetrahedrons. Surprisingly, no CdTe NCs were evident on the apparently clean and smooth exterior surfaces of tetrahedral ZnO in the CdTe/ZnO sample, implying complete encapsulation within the tetrahedron. An increase in the average diameter and size distribution of the chalcogenide QDs in the HSNCs (see Table S1 in the Supporting Information and TEM) indicates that Ostwald ripening takes place during ZnO synthesis at 300 °C.

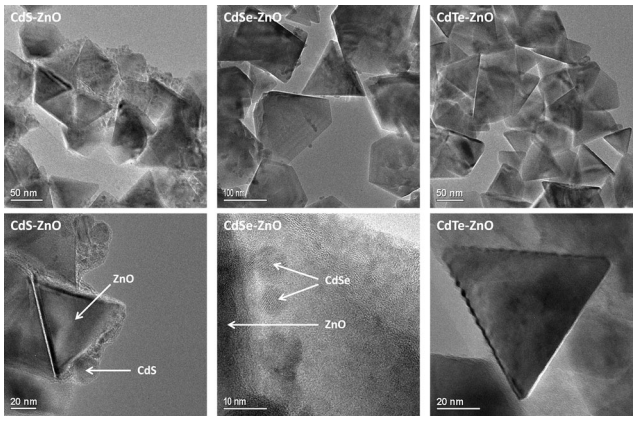

Figure 1. TEM of CdX/ZnO (X = S, Se, Te) HSNCs showing CdS (left) and CdSe (center) decorating the surface of ZnO tetrahedrons, while CdTe (right) is fully encapsulated by ZnO.

X-ray diffraction analysis (XRD) confirms the presence of HSNCs. Intense wurtzite-ZnO diffraction peaks were maintained with no observable peak shifts relative to pure ZnO (Figure 2 A), which indicates that the ZnO phase had not been significantly altered by doping through either cation or anion exchange from the QDs, in contrast to other methods using solution precursors.[14] Distinctive, but less intense, wurtzite-CdS, wurtzite-CdSe, and zinc blende-CdTe XRD peaks were observed (Figure 2 B), indicating that these phases have maintained their own integrity within the composite HSNCs during the ZnO synthesis step. The narrowing of XRD peaks, relative to the pre-synthesized dots, and an increase in the average diameter and size distribution of the cadmium chalcogenide QDs in the HSNCs (see Table S1 in the Supporting Information and TEM) indicates that Ostwald Ripening takes place during ZnO synthesis at 300 °C.

The optical properties of the HSNCs differ significantly from those of pure ZnO. UV/Vis absorption spectra of dry powdered samples clearly indicate absorption edges from the CdX (X = S, Se, Te) phases in the visible region in addition to ZnO band-edge absorption in the UV region ($\lambda \approx 370$ nm) (Figure 3 A). Band-gap values obtained by constructing Tauc plots (Figure S8) indicate that the ZnO NCs, having relatively larger dimensions than the CdX QDs and being the major component of the HSNC, remain unperturbed in the HSNC ensembles. Only a slight decrease of approximately 0.05 eV in the band-edge energy of ZnO was observed for the CdTe/ZnO HSNCs (Table 1), resulting from a small degree of alloying at the materials interface. However the band-gap values of the CdS, CdSe, and CdTe NCs are significantly red-shifted as a result of their extensive contact with ZnO, yielding values of 2.59, 1.93, and 1.52 eV respectively, corresponding to 8.8 %, 14.6 %, and 25.9 % decreases in band-gap energies compared to the as-synthesized CdS, CdSe, and CdTe QDs (see Supporting Information). This red shift may be partially explained by Ostwald ripening, but we believe that it strongly indicates band energy mixing with ZnO at the nano-interface.

Most notably, photocatalytic activity of the HSNCs was significantly increased relative to pure ZnO (for equivalent masses of total catalyst material—that is, approximately 10 % less ZnO by mass for the HSNCs). Photocatalytic activity was assessed using the photodecomposition reaction of the dye methylene blue in aqueous solution under UVA irradiation ($\lambda = 350$ nm; Figure 3 B) after making the catalysts water soluble by a ligand-modification process (Supporting

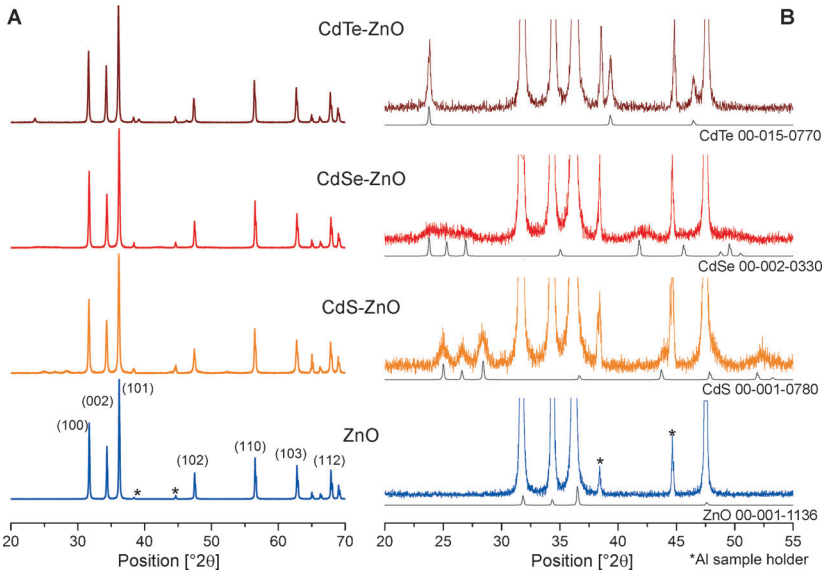

Figure 2. Powder XRD patterns of HSNC nanocrystal ensembles: A) full spectra showing intense wurtzite-ZnO reflections and B) expanded portion of spectra showing less-intense, broader wurtzite-CdS, wurtzite-CdSe, and zinc blende-CdTe peaks.

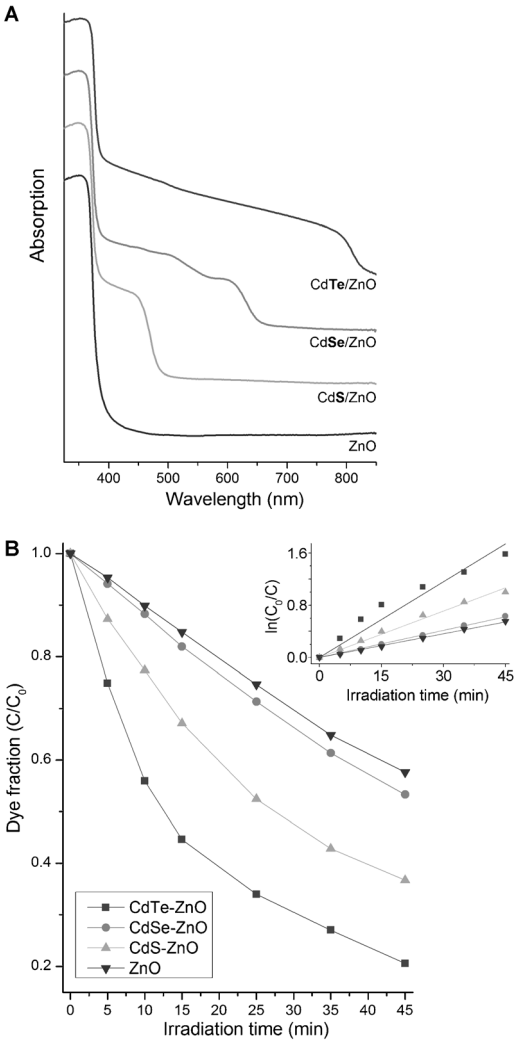

Figure 3. Absorption and photocatalytic profiles: A) Normalized UV/Vis absorption spectra of HSNCs and pure ZnO NCs; B) methylene blue decomposition curves under UVA irradiation ($\lambda = 350$ nm). Inset: Linear plots of pseudo-1st order rate equation. C_0 = initial dye concentration. See Table 1 for *k*-values (slope) obtained from least squares regression analysis.

Table 1: Photocatalytic rate constants (*k*-values) and band-gap values (E_g) for HSNCs and pure ZnO.

Catalyst	*k*-value [min^{-1}]	ZnO E_g [eV]	CdX E_g [eV]
CdTe/ZnO	$0.039 \pm 2.3 \times 10^{-3}$	3.21 ± 0.04	1.52 ± 0.02
CdSe/ZnO	$0.014 \pm 1.4 \times 10^{-4}$	3.26 ± 0.04	1.93 ± 0.02
CdS/ZnO	$0.024 \pm 6.2 \times 10^{-4}$	3.26 ± 0.04	2.59 ± 0.02
ZnO	$0.012 \pm 1.9 \times 10^{-4}$	3.28 ± 0.03	–

Information). Photocatalytic reaction rate constants (*k*-values, Table 1), showed a threefold increase for CdTe/ZnO ($k = 0.039$) followed by a twofold increase for CdS/ZnO ($k = 0.024$), and a slight increase for CdSe ($k = 0.014$) in comparison with ZnO ($k = 0.012$). Each *k*-value was derived from fitted linear pseudo-first order rate equations at room temperature. Surface-area effects were ruled out by observing that the initial uptake of the dye from solution (before irradiation) was constant for all catalysts (ca. 10% uptake). We expect that the dramatic enhancement of the photocatalytic decomposition rate is as a result of an increase in the exciton lifetime and spatial separation because of the establishment of type-II heterojunctions between the cadmium chalcogenide NCs and ZnO. However, the rate order (CdTe > CdS > CdSe) does not seem to follow the band-gap values nor the conduction-band offsets with reference to ZnO. Figure 4 was constructed using relative valence-band

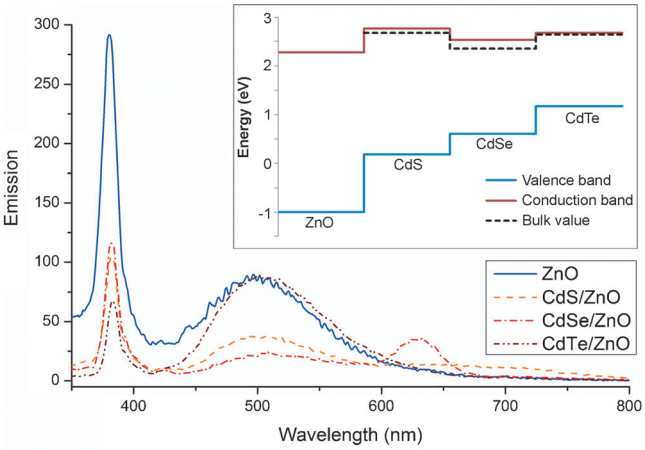

Figure 4. Photoluminescence (PL) emission spectra of HSNCs and pure ZnO in $CHCl_3$ (excitation $\lambda = 280$ nm) normalized according to UV/Vis absorption intensity at $\lambda = 280$ nm. The band-gap peak at $\lambda = 380$ nm and green emission at $\lambda = 500$ nm of ZnO can be seen while the band at $\lambda = 630$ nm is a result of the band-gap emission peak of CdSe (inset: Estimated band-gap offsets for CdX/ZnO HSNCs; X = S, Se, Te).

energies reported by Wei and Zunger[21] along with both experimental E_g values obtained from Tauc plot analysis (Supporting Information) and bulk E_g values. It has been established that binary cadmium chalcogenide CdX (X = S, Se, Te) semiconductor valence bands are mainly composed of filled p-bands of the anion X, with the conduction band composed of empty Cd^{2+} d-bands modulated by mixing with higher unoccupied bands of the anion. Thus, since there is a common cation in all cases, the quantity of excitons generated will depend on the electronegativity of the anion ($X^{-1} \rightarrow X + e^-$). The fundamental Allred–Rochow electronegativity value (χ) is the measure of an element's ability to attract electrons towards itself in a chemical bond and generally decreases down a group in periodic table. Thus, exciton generation ability correlates well with Te(χ=2.01) > S(χ=2.44) > Se(χ=2.48). The alternation pattern in χ with an increase value of Se is as a result of post transition-metal series contraction, which can also be observed in the pattern of conduction-band energies (Figure 4). As a result, the photocatalytic rate enhancement of the HSNC appears to be governed by the ability of the QD to generate excited electrons, which subsequently migrate to the ZnO conduction band and induce redox reactions. Photoluminescence (PL) spectra of colloidal suspensions in $CHCl_3$ (Figure 4) showed a dramatic decrease in ZnO band-gap emission intensity for

the HSNCs relative to pure ZnO, indicating that a substantial amount of photogenerated excitons interact with CdX (X = S, Se, Te) heterojunctions and reduce radiative recombination. Furthermore, the order of this emission attenuation correlates very well with the order of photocatalytic activity: CdTe/ZnO > CdS/ZnO > CdSe/ZnO. It is interesting to note that the intensity of the ZnO green band emission peak at $\lambda =$ 500 nm caused by the presence of structural defects (trap sites) is clearly decreased for CdS/ZnO and CdSe/ZnO HSNCs. We attribute this decrease to the passivation of surface trap sites by CdS and CdSe NCs decorating the surface of ZnO. However, in the case of CdTe/ZnO, this surface trap-site emission of ZnO is maintained without any apparent deactivation, presumably because of the full encapsulation of the CdTe phase (see TEM and ATP).

Atomic probe tomography (APT) was employed to image the spatial characteristics of the nanojunction between the cadmium chalcogenide and ZnO crystalline phases, which is of prime importance for unravelling the fundamental structural basis for efficient charge separation. The 3D spatial reconstruction of single NC samples and junction atomic profiles (Figure 5) clearly indicated heterostructured materials with distinctive nanosized phases of CdX (X = S, Se, Te) in direct contact with ZnO. In agreement with TEM, the atom probe imaging confirmed that regions of Cd^{2+} were situated on the surface of larger Zn^{2+} areas for both CdS/ZnO and CdSe/ZnO samples. However, for a typical CdTe/ZnO sample NC, it was observed that a distinct approximately 15 nm CdTe phase was encapsulated within the ZnO phase. This explains the observations of the presence of CdTe phases in XRD, and the UV/Vis absorption and catalytic results, but its absence on the surface of ZnO according to TEM. XPS gave further evidence for CdTe encapsulation by the extremely low Cd and Te signals (indicating lower surface composition) for CdTe/ZnO (Supporting Information). Closer examination of the composition profile across each HSNC nanojunction by APT (Figure 6) indicated various degrees of ion exchange regions instead of perfectly sharp interface. Cadmium atom mapping across CdS/ZnO, CdSe/ZnO, and CdTe/ZnO heterojunctions revealed diffusion regions into ZnO of approximately 0.5, 1.0,

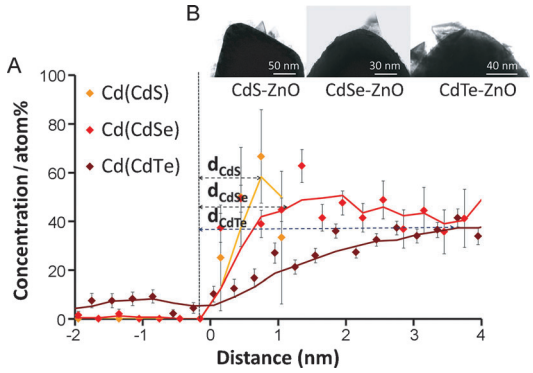

Figure 6. A) Cd atom concentration mapping across ZnO/CdX nanojunction reveals 0.5, 1.0, and 4.0 ± 0.2 nm diffused ion regions with progressive increase in Cd concentration to steady values of CdS, CdSe, and CdTe, respectively; B) HSNC samples immobilized on platinum tip prior to ionization.

and 4.0 ± 0.2 nm. Given lattice mismatches with wurtzite-ZnO of 99.4% (CdTe), 34.8% (CdSe), and 29.6% (CdS), there are considerable strains established at the crystal interfaces. However, these large mismatches do not seem to prohibit epitaxial growth between the two different phases.[22] Ion exchange (alloying) is expected to relax the strain through cross-substitution of ions. The degree of alloying for the QDs is a reflection of their lattice energy or melting point (m.p.). Soft CdTe NCs allow the largest degree of ion exchange with ZnO during the synthesis at 300 °C (m.p. CdTe = 1097 °C; CdSe = 1350 °C; CdS = 1750 °C), accounting for the largest degree of Ostwald ripening and the largest interfacial diffusion region, leading to total encapsulation within ZnO.

To create a high surface semiconductor interface for enhanced photocatalysis, two distinctive NCs of well-defined crystallinity are needed to establish a heterojunction of staggered energy to enable maximum charge separation of excitons. However, the ability of charge movement at their nanosize interface is also crucially important to sustain fast catalytic reactions. It is well understood that excited electrons are far more mobile than holes within crystal lattices. From our APT results, an approximately 4 nm diffusion region at the CdTe/ZnO HSNC interface hosting a gradient of ions between the two nanocrystals is clearly evident. We believe that the atomic arrangement of this nanojunction could also contribute towards a fast hole transport from CdTe to ZnO by electron hopping between adjacent O^{2-} sites

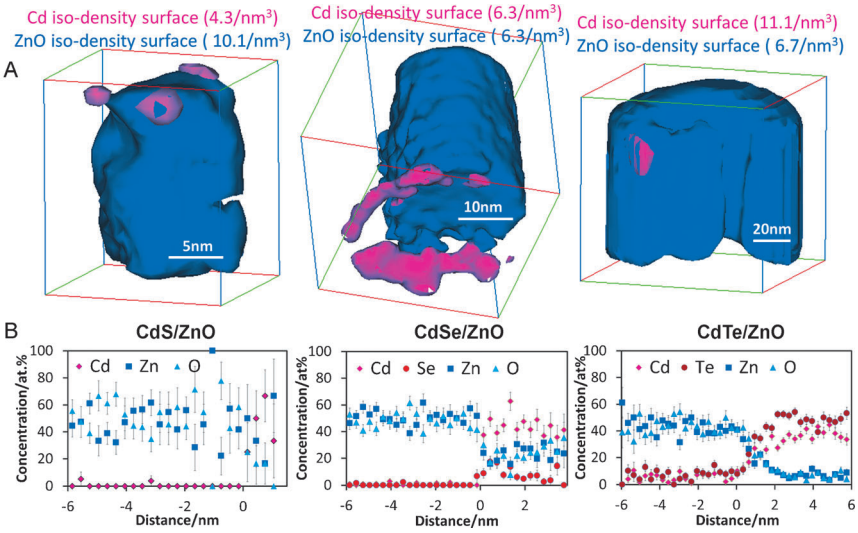

Figure 5. Top: APT three-dimensional spatial reconstruction of Cd^{2+} (pink) and Zn^{2+} (blue) ions present in HSNCs; Bottom: Atomic composition profile of HSNC nanojunction as a function of scanned distance. at.% = atom%. (Note: the overlap of anion peaks in CdS and CdSe with ZnO results in artificially higher ZnO signals; see Supporting Information).

(and also in part Cd^{2+}) that extend across the interface to a wider ZnO surface for photocatalysis. Thus, upon illumination in the visible light region, it is envisaged the excited electrons from CdTe would rapidly transfer to the ZnO conduction band for chemical reduction while the holes in CdTe would be transported to ZnO by electron hopping in the opposite direction against the energy gradient through O^{2-} channels. Additionally, any deeply trapped positively charged hole accumulation within encapsulated CdTe could be quickly relaxed presumably by Auger-type excitations, giving the hole sufficient energy to escape from the valence-band potential well of the CdTe.

In conclusion, we have demonstrated greatly improved photocatalytic activity for the decomposition of aqueous organic molecules under UV/Vis irradiation in novel CdX/ZnO (X = S, Se, Te) HSNCs with well-defined nanojunctions. CdTe is an excellent choice amongst the three QDs investigated as it captures light across the entire solar region, generates the highest number of excitons because of its low anion electronegativity, and its soft ionic nature enables extensive electron and hole movement across a wider alloyed interface for rapid photocatalysis. It is noted that the cadmium chalcogenide-promoted ZnO may still suffer some degree of photocorrosion. However, we did not observe any significant leaching in our short testing time. Thus, the total encapsulation of CdTe in ZnO, forming a crystal within-a-crystal morphology, with a corresponding nanojunction to allow effective charge movement, offers exciting new possibilities in the area of semiconductor-oxide photocatalysis.

Experimental Section

Trioctylphosphine oxide(TOPO)-capped CdS, CdSe, and CdTe nanocrystals (NCs), with diameters between 3–5 nm, were synthesized according to method developed by Peng and Peng.[20] Briefly, CdO and hexadecylphosphonic acid were heated to 320 °C in TOPO under nitrogen to produce organic Cd^{2+} precursors. S-TOP/Se-TOP/Te-TOP precursors, prepared by stirring under inert conditions, were rapidly injected into the Cd^{2+}/TOPO mixture at 270 °C to form NCs, which were then grown at 250 °C for 30 min. Heterostructured CdX/ZnO and pure ZnO NCs were synthesized by a modified procedure based on the method of McLaren et al.[12] CdS, CdSe, or CdTe NCs (10 mg) were loaded into a reaction vessel along with anhydrous zinc acetate (550 mg), oleic acid (3.39 g), and trioctylamine (15 mL). The mixture was degassed under vacuum at 90 °C for 15 min and then heated under nitrogen with stirring to 300 °C for 4 h. Pure ZnO NCs were synthesized by the same procedure, without the addition of any CdS/Se/Te seed NCs. See Supporting Information for details on photocatalytic activity testing and catalyst characterization techniques.

Received: April 19, 2014
Published online: June 24, 2014

Keywords: atomic probe tomography · cadmium · nanocrystals · photocatalysis · semiconductors

[1] M. Curri, R. Comparelli, P. Cozzoli, G. Mascolo, A. Agostiano, *Mater. Sci. Eng. C* **2003**, *23*, 285 – 289.
[2] P. Banerjee, S. Chakrabarti, S. Maitra, B. K. Dutta, *Ultrason. Sonochem.* **2012**, *19*, 85 – 93.
[3] M. Hoffmann, S. Martin, W. Choi, *Chem. Rev.* **1995**, *95*, 69 – 96.
[4] N. Daneshvar, D. Salari, A. Khataee, *J. Photochem. Photobiol. A* **2004**, *162*, 317 – 322.
[5] H. Tong, S. Ouyang, Y. Bi, N. Umezawa, M. Oshikiri, J. Ye, *Adv. Mater.* **2012**, *24*, 229 – 251.
[6] S. Khayyat, M. Abaker, A. Umar, M. Alkattan, N. Alharbi, S. Baskoutas, *J. Nanosci. Nanotechnol.* **2012**, *12*, 8453 – 8458.
[7] L. Chen, Y. Tu, Y. Wang, R. Kan, C. Huang, *J. Photochem. Photobiol. A* **2008**, *199*, 170 – 178.
[8] F. Peng, H. Zhu, H. Wang, H. Yu, *Korean J. Chem. Eng.* **2008**, *24*, 1022 – 1026.
[9] P. Li, Z. Wei, T. Wu, Q. Peng, Y. Li, *J. Am. Chem. Soc.* **2011**, *133*, 5660 – 5663.
[10] C. Yu, K. Yang, Y. Xie, Q. Fan, J. C. Yu, Q. Shu, C. Wang, *Nanoscale* **2013**, *5*, 2142 – 2151.
[11] Y. Haldorai, J.-J. Shim, *Compos. Interfaces* **2013**, *20*, 365 – 377.
[12] A. McLaren, T. Valdes-Solis, G. Li, S. C. Tsang, *J. Am. Chem. Soc.* **2009**, *131*, 12540 – 12541.
[13] D. Li, H. Haneda, *Chemosphere* **2003**, *51*, 129 – 137.
[14] F. Liao, Z. Zeng, C. Eley, Q. Lu, X. Hong, S. C. E. Tsang, *Angew. Chem.* **2012**, *124*, 5934 – 5938; *Angew. Chem. Int. Ed.* **2012**, *51*, 5832 – 5836.
[15] M. Lee, K. Yong, *Nanotechnology* **2012**, *23*, 194014.
[16] X. Huang, L. Shang, S. Chen, J. Xia, X. Qi, X. Wang, T. Zhang, X.-M. Meng, *Nanoscale* **2013**, *5*, 3828 – 3833.
[17] V. Consonni, G. Rey, J. Bonaimé, N. Karst, B. Doisneau, H. Roussel, S. Renet, D. Bellet, *Appl. Phys. Lett.* **2011**, *98*, 111906.
[18] Y. Liao, W. Que, J. Zhang, P. Zhong, Y. Yuan, X. Qiu, F. Shen, *J. Nanosci. Nanotechnol.* **2013**, *13*, 959 – 963.
[19] F. Xu, V. Volkov, Y. Zhu, H. Bai, A. Rea, N. V. Valappil, W. Su, X. Gao, I. L. Kuskovsky, H. Matsui, *J. Phys. Chem. C* **2009**, *113*, 19419 – 19423.
[20] Z. Peng, X. Peng, *J. Am. Chem. Soc.* **2001**, *123*, 183 – 184.
[21] S.-H. Wei, A. Zunger, *Appl. Phys. Lett.* **1998**, *72*, 2011 – 2013.
[22] J. Jaffe, T. Kaspar, T. Droubay, T. Varga, *J. Vac. Sci. Technol. A* **2013**, *31*, 061102 – 061109.